DOI: 10.31276/VJSTE.65(4).54-61

Investigation of residual stress in epoxy-based coatings using X-ray and FEM-ANN techniques

Jasim Haider Hadi*

University of Basrah, Basra City, Iraq

Received 30 January 2023; revised 12 February 2023; accepted 3 October 2023

Abstract:

Residual stresses play a significant role in the properties and performance of epoxy-based coatings, with their origins rooted in various factors encountered during production and application. This study focuses on quantifying residual stresses in three distinct epoxy-based coatings, commonly used as linings for crude oil storage tanks, namely, pure epoxy, Novolac epoxy, and glass-flake-reinforced epoxy. We employ X-ray diffraction to measure these residual stresses and compare them against predicted values obtained through finite element and artificial neural network methods. Our findings reveal notable differences in residual stresses among the three types of epoxy coatings. Specifically, pure epoxy coatings exhibit higher residual stresses, Novolac epoxy coatings display the lowest, and those reinforced with glass flakes fall in between. Utilising the FEM-ANN model for simulations yields results that closely align with experimental measurements obtained via the X-ray method. Test results demonstrate that the coatings cured at high temperatures have high residual stresses compared to those cured at lower temperatures. Increasing the curing temperature from 10 to 50°C will increase residual stresses by 40.81, 11.085, and 56.98% for coatings reinforced with glass-flake, Novolac, and pure epoxy-based coating, respectively.

Keywords: **curing temperature, glass-flakes, residual stress, volumetric shrinkage, X-ray method.**

Classification numbers: **2.2, 2.3**

1. Introduction

Epoxy coatings consisting of two components, a base and a hardener, are commonly employed for safeguarding crude oil storage tanks, ensuring their continued operational performance. However, a range of factors, including intrinsic characteristics, thermal influences, volumetric changes, and lattice disparities, can introduce residual stress into these epoxy coatings, potentially compromising their performance [1]. Throughout the crosslinking and curing process, volumetric transformations occur, driven by the interaction between the base and the hardener [2]. The presence of fillers, fibres, or glass flakes can exacerbate this issue as these materials often shrink at different rates compared to the resin and hardener, leading to the formation of residual stresses. Furthermore, parameters such as curing temperature and coating thickness significantly impact the initiation of residual stresses during the curing process of epoxy-based coatings [3]. Intrinsic residual stresses may also be present, stemming from defects like air bubbles and grain boundaries within the epoxy coating [4].

Various methods are employed to evaluate residual stresses, encompassing both experimental and numerical techniques [5]. The X-ray diffraction (XRD) technique is widely utilised for measuring residual stresses in diverse materials. XRD assesses strain within the crystal lattice, allowing for the calculation of residual stress based on elastic constants [6]. In contrast, numerical methods such as finite element method (FEM) and artificial neural networks (ANN) have gained popularity for predicting residual stresses. FEM entails complex non-linear analyses, influenced by boundary conditions and modelling procedures [7, 8], while ANN, as a computational model, employs artificial neurons to simulate structural organisation, predict relationships between input parameters, and model the system [9, 10].

Despite the critical implications of residual stresses, their evolution within epoxy coatings has received limited research attention. P. Kamarchik, et al. (1980) [11] reviewed the application of the X-ray technique for measuring and estimating residual stresses in coating and coating-related systems. The results indicated that less adhesion and misleading cross-linking between coating molecules can result from the residual stresses. I. Kishore (2003) [12] used finite element analysis to simulate the formation of residual stress in epoxy resins created due to the influence of dimensional constraints. The simulation results indicate that there are possible areas where delamination and cracking in epoxy

*Email: ashaqqu73@gmail.com

can occur, and the residual stress in epoxy resins is generated from volumetric changes that occur throughout the curing and crosslinking process. S.B. Aboubakar (2009) [13] computed and analysed residual stresses at fibre-epoxy interfaces using an axisymmetric model. Two cases are considered, an epoxy matrix with glass and carbon fibres respectively with different fibre volume. The results show that the stresses at the interface are affected by residual thermal stresses, particularly in the free edges. J. Cheng, et al. (2009) [14] synthesised and studied the curing temperature and thermal stability of novel epoxy coatings containing 4,4-diaminodiphenyl sulfone as a hardener and 4,4-diaminodiphenylmethane as a base using differential scanning calorimetry. They found that the thermal decomposition temperature of epoxy coatings increased with the increase in curing time and the rise in curing temperature. M. Frantisek, et al. (2014) [15] developed a new approach using a neural network method to analyse residual stresses and compared their results with that obtained from the experimental C-Ring measurement method. It has been shown that the neural network method is a good procedure for the analysis of residual stresses. D. Taisei, et al. (2015) [16] measured the residual stress in polyamide film polymer using the X-ray diffraction technique. The diffractometer with a transmission method was used in experimental measurement. They discussed the problems related to measuring residual stresses in polymer coatings and showed that the X-ray technique is a good method to measure residual stresses in polymer coatings. Q. Li, et al. (2022) [17] studied the internal stresses in epoxy coatings using both analytical and experimental methods, including the attenuated total reflection-fourier transform infrared technique and dynamic mechanical thermal analysis. They investigated the effect of various parameters, including the molecular structures of binders and hardeners, filler type and concentration, and initial solvent concentration on internal stress values.

In our study, we focus on measuring the residual stress in three types of Hample epoxy coatings, namely pure epoxy, Novolac epoxy, and epoxy reinforced with glass fibres. These coatings find application in crude oil storage tank linings. We employ X-ray diffraction to measure residual stresses and compare the results with those calculated using the FEM-ANN method. Our investigation delves into the impact of coating thickness, volumetric shrinkage, coating viscosity, and curing temperatures, simulating these variables using FEM-ANN techniques.

2. Materials and methods

2.1. Experimental procedure

2.1.1. Types of epoxy coatings

Three types of Hampel epoxy coatings have been used for studying. These types are commonly used for covering crude oil storage tanks in South Iraq. These coatings consist of two parts (base and hardener) which are in the liquid state and mixed together before being applied to the steel surface. These coatings are: (1) HEMPADUR 15600, amine adducts cured pure epoxy coats. The mixed volume ratio is 1:1 of base to hardener. Thickness of coatings ranges from 160-200 µm. Refer to this coat as model A; (2) HEMPADUR 85671, this is a two-component solvent-free amine-cured phenol Novolac epoxy coating. The volume ratio of mixing is 1:2 of base epoxy to hardener. The thickness of this coating is in the range of 250-600 µm. Refer to this type of coats as model B; (3) HEMPADUR multi-strength GF-35870 is an amine-adduct cured epoxy coating, the coats are reinforced with glass-flakes. The mixing volume ratio is 3:1 of base to hardener. The maximum thickness of coatings is 350 µm. Refer to this type of coats as model C.

These types of Hampel epoxy-based coatings are manufactured by Sharjah Coating Company, U.A.E., and they are used as manufactured for plain coating of tanks without external additives except model C is reinforced by glass fibre as produced by the company.

2.1.2. Specimen preparation and coats

The 3×3 cm samples with a thickness of 6 mm were used of ASTM A537 C1 carbon steel which was widely applied in the building of crude oil storage tanks of South Iraq. The specimen dimensions are considered according to ASTM-E0915-96R02 [18]. The chemical compositions of ASTM A537 carbon steel as a percentage are Fe: 97.58, C: 0.24, Mn: 1.6, P: 0.035, S: 0.035, Cr: 0.025, Si: 0.5, Mo: 0.8, Ni: 0.25, Cu: 0.35 [19]. Fig. 1 shows specimens before and after coatings in addition to SEM image (100 times magnified) of the cross-section to show the thickness of epoxy coatings. All Hampel coatings were applied by airless spray to steel substrates at nominally standard film thicknesses as given by the manufacturing company. The PosiTector 6000 coating thickness gauges manufactured by LABOMAT (France) were used to check the coating thickness.

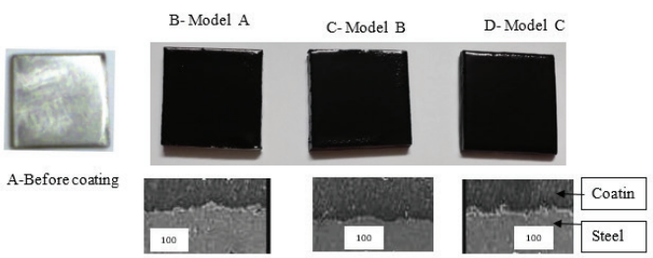

Fig. 1. Specimens before and after coatings with SEM image.

To study the effect of curing temperature on the residual stresses induced during solidification, the samples of the three models of coatings were left to cure at nine temperatures (10, 15, 20, 25, 30, 35, 40, 45 and 50°C), respectively. Based on information provided in the manufacturer's data sheets for various types of epoxy-based coatings, the curing time for model A is up to 72 hours, the curing time for model B is 7 days, and the curing time for model C typically takes 10 days. A total of 100 specimens were used for X-ray measurement.

2.1.3. Residual stress measured by X-ray

In X-ray diffraction (using the $\sin^2 \psi$ method), the strains in the crystal lattice of the coatings were measured along the tangential direction, and the associated stress is computed from the elastic constants (modulus of elasticity and Poisson's ratio) assuming a biaxial state of stresses [20]. The basic assumption throughout strain measurement by X-ray diffraction is that the plane of the crystal lattice in epoxy-based coating has a uniform linear elastic distortion. The d-spacing was measured by a diffractometer for different values of ψ, and the residual stress is calculated using the following relationship [21]:

$$\sigma_{res.} = \frac{E}{(1+\nu)\sin^2(\psi)} \frac{d_\psi - d_n}{d_n} \quad (1)$$

where d_ψ is the inter-planar spacing of planes at an angle ψ to the surface (μm); d_n is the inter-planar spacing of planes normal to the surface (μm); E is the elastic modulus of the coatings (GPa), ν is Poisson's ratio; ψ are the angles through which the sample is rotated.

Table 1. List of specification of X-ray diffraction.

Specification	Values
Chart speed	15 mm/min
Incident angle of X-ray	0,18,36,45
Gonio scan speed	1 deg/min
Divergent angle	0.35 deg
Irradiation area	3×3 mm²
Time constant	5 sec
Tube current	15 mA

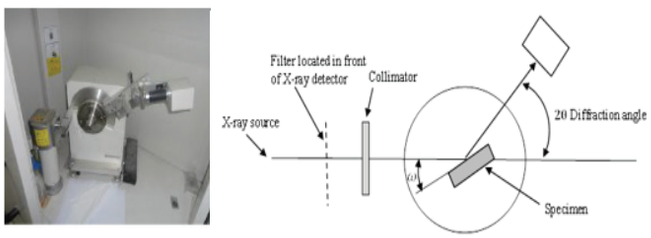

(A) X-Ray diffraction machine (B) Method of measured residual stresses

Fig. 2. X-Ray diffraction machine and method of measured residual stresses using X-ray diffraction.

The X-ray measurements were performed on an ADX-8000 Mini θ-θ Powder X-ray diffraction instrument manufactured by Angstrom Advanced Inc. The X-ray source is a Cu tube, which is used for all specimens tested. Since the thickness of epoxy coats is relatively small, and only the surface strain can be achieved. The goniometer was used to read and record the angle (2θ). The collimator was used to control the irradiated area. Table 1 lists the specifications used by X-ray diffraction. X-ray diffraction experiments were conducted using the machine illustrated in Fig 2A at the Ministry of Science and Technology. A voltage of (10 kV) and a current of 15 mA were supplied to the target, which is copper with a wavelength of 1.5406 Å, and nickel as the filter material. Fig 2B shows the method of measured residual stresses.

Table 2. Epoxy coating elastic modulus and Poisson's ratio obtained from tensile test.

Cure temperature °C	Elastic modulus (GPa.)			Poisson's ratio		
	Model A	*Model B*	*Model C*	*Model A*	*Model B*	*Model C*
10	2.24	1.65	0.96	0.42	0.31	0.27
15	2.20	1.61	0.95	0.42	0.31	0.27
20	2.18	1.60	0.94	0.43	0.34	0.28
25	2.15	1.59	0.91	0.43	0.34	0.28
30	2.14	1.57	0.89	0.40	0.34	0.28
35	2.12	1.55	0.88	0.40	0.35	0.28
40	2.11	1.52	0.85	0.45	0.35	0.28
45	2.10	1.51	0.84	0.45	0.35	0.29
50	2.10	1.50	0.83	0.45	0.35	0.29

To compute the residual stress from Eq. (1), the unstressed lattice spacing d_n, the stressed lattice spacing d_ψ, the elastic modulus and Poisson's ratio of epoxy-based coatings must be determined. Different methods for obtaining the unstressed and stressed lattice spacing are found. Due to simplicity, the $sin^2\psi$ method is used for determining d_n and d_ψ lattice spacing. A number of X-ray measurements are performed to determine the interplanar spacing (d_n) in μm for various values of ψ. Then, a linear curve of d vs. $sin^2\psi$ is plotted, and the value of the lattice spacing is intercepted on the y-axis at $sin^2\psi$ = 0, which is considered d_n [22]. The two common causes of error that affect XRD results are specimen- and instrument-sensitive errors. The best precision attainable for the machine used is about +0.4%, and the probable error does not exceed +1% according to the manufacturing data sheet. The samples were sent for measuring the residual stresses immediately after curing at each temperature.

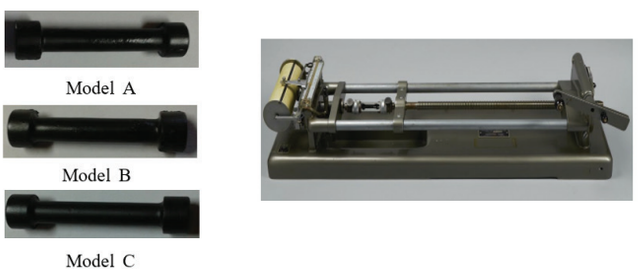

Fig. 3. Epoxy coating specimens for tensile testing and tensile testing machine.

The measurement of mechanical properties (e.g., elastic modulus and Poisson's ratio) of the epoxy coating has some difficulties because the structure of epoxy coatings is complex and contains lamellae, pores, micro-cracks, and so on. The Hounsfield hand-operated universal tensile testing machine SM1002, Hounsfield Company, UK), in accordance with ASTM E8M-01 [23] and ASTM D638-14 [24], shown in Fig. 3, is used for achieving tensile tests to measure the elastic modulus and Poisson's ratio of the three types of epoxy coatings. Two strain gauges were used, one to measure longitudinal deformation and the other to measure contraction in the median of the specimen during the test.

Figure 3 shows specimens after moulding and solidification. Two glass plates with dimensions and shape similar to the tensile test specimen given by ASTM E8M-01 and ASTM D638-10 [23, 24] were used as moulds for casting the three Hample epoxy coatings to prepare the tensile specimens. Rubber binding around the glass plates was used to fix them. The specimens were left to cure at temperatures (10, 15, 20, 25, 30, 35, 40, 45, and 50°C). The specimen has a 50 mm gauge length and 5 mm diameter. The specimens are treated as elastic materials for tensile tests. A total of 54 specimens were prepared for tensile testing.

2.2. Numerical methods

2.2.1 FEM

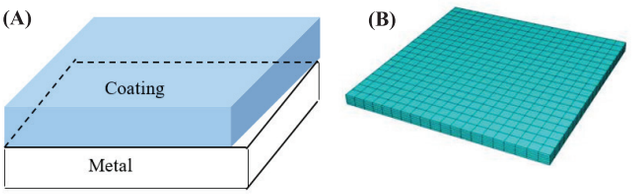

Fig. 4. The meshes used in the models. (A) Metal-coating system; **(B)** Finite element mesh of coating.

FEM was carried out using the commercial software ANSYS V.7 for both thermal and displacement analysis. The coatings were modelled in 3D with 8-node quadratic quadrilateral elements. The meshes used in the models are shown in Fig. 4. The boundary conditions for the models state that all nodes on the top surface are subjected to temperature (10, 15, 20, 25, 30, 35, 40, 45, and 50°C), while bottom surface nodes are constrained in the X-Y directions.

The finite element analyses were carried out on 3D models using temperature-dependent material properties: elastic modulus and Poisson's ratio. The elastic modulus and Poisson's ratio are determined from tensile test specimens cured at various temperatures. The reference coefficient of thermal expansion (CTE) is 70×10^{-6}/°C for amine-cured phenol Novolac epoxy, while for amine-adduct cured pure epoxy paint, it is about 121.4×10^{-6}/°C, and for amine-adduct cured epoxy coating reinforced with glass flakes, it is about 30×10^{-6}/°C at room temperature according to company manufacturing data sheet information. For other temperatures, the coefficient of thermal expansion used in ANSYS V.7 software program is calculated using the Eq. [25]:

$$\alpha_T = \frac{\ln(\alpha_{ref}*(T-T_{ref})+1)}{(T-T_{ref})} \quad (2)$$

where α_T is the coefficient of thermal expansion at temperature T, T is the temperature (°C), α_{ref} is the reference coefficient of thermal expansion, a value of 0.01 in this analysis, and T_{ref} is the reference temperature for thermal expansion, usually taken as 22°C.

There are 2000 elements in the FEM analysis, each with a size of 0.0065 mm.

2.2.2. Artificial neural networks

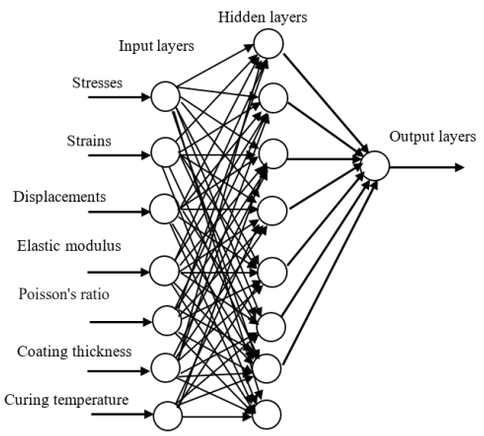

Fig. 5. Schematic diagram of ANN method for predicting residual stresses.

For the predictive analysis using ANN, the ANN model consists of three layers: the input layer, the hidden layer, and the output layer [26]. The input parameters for the ANN model consist of the strains and displacements obtained from the numerical simulations using FEM, with mechanical properties obtained from tensile tests, and the outputs are the corresponding predicted residual stress. The learning function is the gradient descent algorithm with momentum weight and bias learning functions. The number of hidden layers and neurons are determined through a trial-and-error method to accommodate the convergence error. The structure of the proposed ANN model is 7 neurons in the input layer, 1 neuron in the output layer, and the number of neurons in the hidden layer was obtained by trial testing from 10 to 20 neurons using the Levenberg-Marquardt (LM) learning algorithm. The learning rate is 0.55, with a momentum term of 0.9, and the network training consists of 10,000 iterations. The error between the desired and actual output is less than 0.001 at the end of the training process. Fig. 5 shows the basic architecture of the artificial neural network model. MATLAB R2010b with the neural network toolbox was used during the studies for training and testing data obtained from FEM and tensile tests. The root mean square error (RMSE) and correlation coefficient (R^2) values were used for comparison [9]:

$$RMSE = \left[\left(\frac{1}{n}\right)\sum_j \left|t_j - o_j\right|^2\right]^{1/2} \quad (3)$$

$$R^2 = 1 - \left(\frac{\sum_j (t_j - o_j)^2}{\sum_j (o_j{}^2)}\right) \quad (4)$$

where t is the goal value; o is the output value, j is the sampling point, and n is the number of samples. The standard error (uncertainty) can be determined by calculating the mean stress using the following equation [9]:

$$\sigma_m = \frac{(\sigma_1 + \sigma_2 + \cdots.)}{N} \quad (5)$$

where N is the number of data points, m is the mean of stresses.

The standard deviation can be given by:

$$\sigma_{standard} = \sqrt{\frac{(\sigma_i - \sigma_m)^2}{N-1}} \quad (6)$$

and the standard error is evaluated by:

$$\sigma_{error} = \frac{\sigma_{standard}}{\sqrt{N}} \quad (7)$$

3. Results and discussion

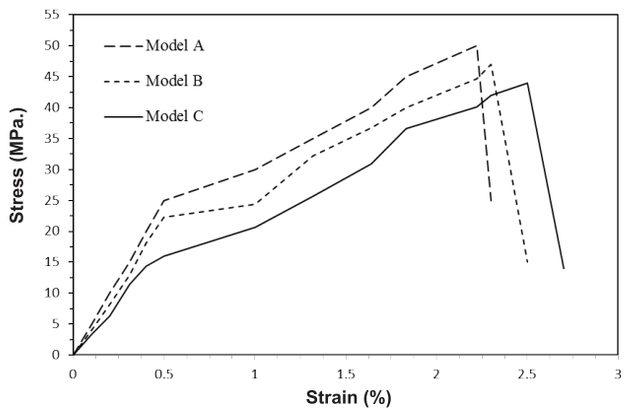

Fig. 6. The stress-strain curves of epoxy coatings cured at 10°C.

Figure 6 shows stress-strain curves of the three Hample epoxy coatings cured at 10°C obtained from tensile tests of specimens given in Fig. 3. The thickness of each sample differs from others but is within the range of thickness given by the manufacturer's data sheets. As illustrated in Fig. 6, there is a linearly elastic response of the stress-strain curves until the point of maximum stress, followed by abrupt failure at strains larger than 2.28, 2.47, and 2.68% for models A, B, and C, respectively. Elastic modulus was extracted from the stress-strain curves of Hample epoxy specimens cured at various temperatures, while Poisson's ratio is determined from longitudinal and lateral strain measured by strain gauges during the test. The behaviour of the three epoxy coatings is similar to metallic materials, as indicated in all stress-strain curves, i.e., the tensile strength increased with increasing load until failure. The tensile test is conducted for the similar tensile test specimens cured at temperatures (15, 20, 25, 30, 35, 40, 45, and 50°C). Similar curves are obtained and used for determining the elastic modulus and Poisson's ratio at these curing temperatures. Table 2 summarises the elastic modulus and Poisson's ratio for the three models of epoxy coatings at different curing temperatures. The yield strength is obtained by the 0.2% offset yield strength. This is used as points to obtain elastic modulus and Poisson's ratio. When taking 30 points arbitrarily from curves in Fig. 6, the uncertainty error analysis using Eqs. 5-7 show that the error in data obtained from tests is less than 0.1%.

As indicated in Table 2, model C has lower values of elastic modulus and Poisson's ratio due to its rigidity because of reinforcement by glass flakes compared to others. Also, the effect of increasing curing temperature on elastic modulus values is less compared to other types of coatings. For model A and B, the values of elastic modulus have a high effect on curing temperature, and the modulus reduces as curing temperature increases. The effect of curing temperature on values of Poisson's ratio is very small compared to the effect on the values of elastic modulus.

All data obtained from the tensile test in Table 2 are parameters input to FEM programs. The displacements and strains in each element of the coating surface system are obtained by solving the *n* independent equations resulting from FEM meshes in the three-dimensional case. In the finite element analysis, the boundary temperatures are set at curing temperature 10°C and then increase by step increments of 5°C for each case of calculating displacement and strains. The FEM results, in addition to cure temperature and coating thickness, are inputs to the neural network toolbox of MATLAB R2010b and used to train the ANN model that is shown in Fig. 5.

By training several networks and estimating the error, the optimal number of neurons in the hidden layers is determined. Trials were conducted using two learning algorithms, the Levenberg-Marquardt learning algorithm (LM) and resilient backpropagation (RP). The trials conducted that the LM learning algorithm to be the best one for the residual stresses. Table 3 presents the optimal number of neurons in hidden layers for residual stresses. According to Table 3, the best input layers, hidden layers, and output layers are 7-13-1. The Log-sigmoid transfer function is used for training the input data in the hidden layer with backpropagation algorithm. The predicted residual stresses were validated with that obtained from the X-ray method.

Table 3. Statistical data of residual stresses for 10 learning algorithms.

Learning algorithm	Number of neurons	Training data		Testing data	
		RMSE	R^2	*RMSE*	R^2
LM	7-10-1	0.1043	0.9632	0.0930	0.9540
LM	7-11-1	0.1047	0.9678	0.0962	0.9483
LM	7-12-1	0.0944	0.9555	0.0931	0.9644
LM	**7-13-1**	**0.0845**	**0.9110**	**0.0882**	**0.9514**
LM	7-14-1	0.0946	0.9473	0.0931	0.9453
RP	7-15-1	0.0959	0.9337	0.0945	0.9588
RP	7-16-1	0.0924	0.9550	0.0950	0.9633
RP	7-17-1	0.0980	0.9588	0.0828	0.9623
RP	7-18-1	0.1075	0.9578	0.0910	0.9468
RP	7-19-1	0.1081	0.9589	0.0942	0.9394

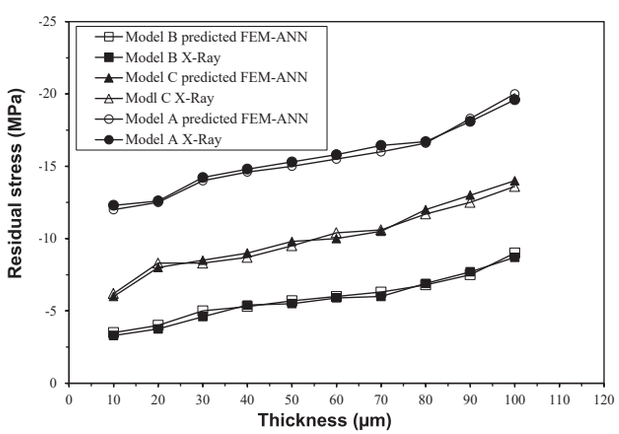

Fig. 7. Variation of residual stresses with thickness at 10°C.

Figure 7 compares the residual stresses of the three types of epoxy coatings cured at 10°C as a function of coating thickness. It also compares those measured using the X-ray method at the centre of coated specimens and those calculated by the FEM-ANN method at room temperature. As indicated, the results appear to be in excellent agreement. The residual stresses in the radial direction are very small, so they are neglected, and the stresses in the tangential direction are considered only.

The maximum residual stresses for epoxy coatings obtained from the X-ray measurements are -20.9, -9.11, and -14.04 MPa for coatings A, B, and C, respectively. While those obtained from the FEM-ANN method are -19.57, -8.72, and -13.61 MPa for coatings A, B, and C, respectively. The magnitude of the residual stresses is lower at the interface region of samples and begins to increase with coating thickness increases. The increase in coating thickness increases the time needed to cure the coatings, and this leads to an increase in reactions between base and hardener to form the crosslink density of epoxy coatings. This leads to an increase in the values induced by stresses. Also, it can be noted that the residual stress distribution induced in a coating layer is not uniform through thickness and varies due to different types of compositions and reinforcement. Also, it can be noted that all residual stresses are compressive stresses. As seen, the compressive residual stress would be produced because the reaction between base and hardener during mixing to produce epoxy coating was completely occurs after coating applied. Also, the residual stress in the epoxy coating is compressive due to the smaller coefficient of thermal expansion of the epoxy coat than that of the substrate of steel coated.

Model A consists of amine adduct cured pure epoxy paint which has a high content of residual solvents, monomers, and low molecular weight extractables that induce high residual stress compared to models B and C. model C is reinforced by glass flakes, and this reduces the internally induced stresses.

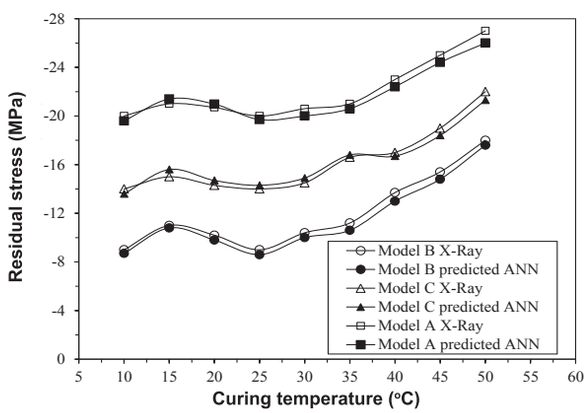

Fig. 8. Variation of residual stresses with curing temperatures.

Figure 8 shows a comparison of residual stresses obtained from X-ray measurement and the FEM-ANN method as a function of curing temperatures at a thickness of 100 µm. The temperatures selected for study range from 10 to 50°C, increasing by steps of 5°C. From Fig. 8, the residual stress value has a major influence on the solidification temperature of the epoxy-based coating. The residual stresses acquired from X-ray diffraction at 10°C and a thickness of 100 µm are -19.60, -9.11, and -14.04 MPa for models A, B, and C, respectively, while values obtained from FEM-ANN methods are -19.57, -8.72, and -13.61 MPa for models A, B, and C, respectively. The residual stresses acquired from X-ray diffraction at 50°C and a thickness of 100 µm are -27.11, -18.10, and -22.04 MPa for models A, B, and C, respectively, while those obtained from FEM-ANN methods are -26.05, -17.61, and -21.30 MPa for models A, B, and C, respectively. This shows that there is a significant increase in residual stress values with an increase in curing temperatures of coatings, whereas these values are lower at lower temperatures. It is found from Fig. 8 that the best curing temperature is 25°C, which provides a lower value of residual stress. From these results, it is demonstrated that the residual stresses generated will increase by percentage values of 40.81, 11.085, and 56.98% for models A, B, and C, respectively, when the curing temperature rises from 10 to 50°C.

In the case of amine adduct cured pure epoxy coating, if the curing temperature is low, it leads to low reactivity of the amine group when mixing with the epoxy. This causes an excess of epoxy rings in the backbone and results in fluctuations in the curing rate or solidification rate of coatings, making the cure mechanism difficult. This process induces high residual stress compared to other types. However, a high curing temperature may accelerate the reactivity of amine hardeners and reduce the time of solidification. In other words, increasing cure temperatures increase the evaporation of hardener (exothermic reactions or increase activation energy between base and hardener), which leads to an increase in the values of residual stresses induced. Also, if the thickness of the coating increases and the curing temperature rises, this makes the coatings soft and more flexible due to the heat not escaping or dissipating as easily. Thus, increases in residual stresses with the thickness of coatings.

One of the most important properties of epoxy coatings influenced by curing temperature is the cross-linking density of the epoxy coats and its process, and this directly affects the values of initiated residual stress. A very dense cross-linking between coating components forms a very strong network through the epoxy coating and enhances its mechanical properties. In the case of model B, which contains Novolac coats, the Novolac epoxy coating results from the reaction of phenol functional groups (hardener) and formaldehyde resin (base). After the mixing process, the curing process results in a very cross-linked material. During cure, the cross-link density of Novolac epoxy coating increases gradually, transforming the liquid reactants into a solid to yield an amorphous solid. As the physical state of the Novolac coating changes during cure, it experiences residual stresses due to volume shrinkage and the effect of the curing temperature.

For model C, as the curing temperature rises, thermal expansion causes a decrease in tension on the glass flakes and an increase in compression of the epoxy matrix. Due to the difference in the coefficient of expansion between the glass flakes and

the epoxy matrix, the induced residual stresses are rather small compared to model A. For coating C, the coatings have medium values of compressive residual stresses, but they have high densities compared to the other types of coatings. On the other hand, in the glass flake/epoxy systems, residual stress develops during thermal cure due to the shrinkage of the epoxy. The cure shrinkage between the glass flakes and epoxy base is less at lower curing temperatures compared to elevated ones, which also leads to an increase in crosslink density and reduces initiated stresses. However, the shrinkage due to chemical curing and crosslinking of the Novolac epoxy is larger than that of model C coatings.

To make a comparison between the volumetric shrinkage of the tested epoxy coatings, the volumetric shrinkage of the three epoxy coats was calculated using the following equation [27, 28]:

$$\text{Volumetric shrinkage } (\%) = -\frac{\rho_u}{\rho_c} \times 100\% \quad (8)$$

where ρ_u is the density of the uncured epoxy coatings (kg/m^3) and ρ_c is the density of the curing epoxy coatings (kg/m^3).

The density of curing epoxy coats was determined experimentally using a simple method on a cylindrical specimen. A cavity is made on the specimen, following which the epoxy coats are sprayed on it. After spraying, the coating is ground to make this specimen cylindrical. Given the known size of the substrate, the volume of the coating can then be calculated. After the specimen is ground and weighed, the coats are ground to obtain the mass of the coating [29]. Table 4 shows the density of uncured epoxy coats which is given by data sheets of the manufacturer's company [30-32] and those calculated by using a direct method for curing epoxy coats.

The values of volumetric shrinkage calculated for the three models are 5.10, 3.73, and 4.55% for models A, B, and C, respectively. Model A, containing amine adduct pure epoxy coatings, shows a large volume shrinkage upon curing, while model B shows low shrinkage during the curing process, and model C shows a moderate value.

The reinforcement occupies a small position in epoxy coats and is formed from local shrinkage during the curing of the epoxy and hardener reactions, acting as a bridge interconnecting coating molecules. This results in reduced volume shrinkage in addition to an increase in cross-linking density [33]. The formation of voids in the cured amine adduct pure epoxy coats occurs due to the volume shrinkage during the curing reaction, resulting in an increase in the inducing internal stresses in these coats [34]. The volume shrinkage has conventionally been reduced by the addition of organic and inorganic reinforcement. However, the addition of reinforcement to curable compositions frequently results in an increase in viscosity and thus reduces fluidity [35, 36].

At low temperatures, the base-hardener epoxy coating cure reaction proceeds very slowly compared to that at high temperatures, affecting the values of initiated stresses. At 20°C, the reaction becomes stable compared to other temperatures, leading to smaller initiated residual stresses compared to other curing temperatures. The results show that the tangential residual stress at high curing temperatures is higher for the three models of epoxy coat when compared to lower curing temperatures.

Compared to the amine adduct curing epoxy, the Novolac coating has greater viscosity. The amine adduct curing epoxy has lower reactivity when reacting the epoxy resin with hardeners, which reduces the curing process of this type of coating [37]. The chemical backbones of Novolac epoxies have more reactive groups (functionality) which can result in higher curing temperature and a highly cross-linking density compared to amine cure pure epoxy coat. This highly chemical cross-linking enhances the thermal and chemical resistance of the coating [38]. As the curing process is slow with time, the residual stress created is increased due to the increased cure time. Adding glass flakes to model C increases the crosslink density but has also been found to increase the residual stress compared to model B.

4. Conclusions

This study has investigated the influence of curing conditions and epoxy coating thickness on residual stress values. The discussion has highlighted a strong agreement between X-ray diffraction and the FEM-ANN model in assessing residual stresses. Curing temperature, in particular, has emerged as a key factor, with lower curing temperatures resulting in reduced residual thermal stresses compared to higher temperatures. Specifically, the results indicate that at 10°C, the residual stresses measured by X-ray diffraction are -19.60, -9.11, and -14.04 MPa for models A, B, and C, respectively. Correspondingly, the values obtained from the FEM-ANN methods are -19.57, -8.72, and -13.61 MPa for models A, B, and C, respectively. Similarly, at 50°C, the residual stresses recorded by X-ray diffraction are -27.11, -18.10, and -22.04 MPa for models A, B, and C, while the FEM-ANN methods yield -26.05, -17.61, and -21.30 MPa for the same models. Importantly, regardless of the assessment method, all residual stresses are found to be compressive.

Furthermore, the investigation reveals that residual stresses exhibit variation across the coating thickness. For instance, at a thickness of 10 μm, the residual stresses determined by X-ray diffraction and FEM-ANN methods are -11.97, -3.52, and -6.25 MPa for coatings A, B, and C, respectively. When the thickness is increased to 100 μm, the corresponding values are -20.9, -9.11, and -14.04 MPa for coatings A, B, and C using X-ray diffraction, and -19.57, -8.72, and -13.61 MPa for the same coatings using the FEM-ANN method.

In summary, model B, consisting of free amine-cured phenol Novolac epoxy, displays lower residual stress values. Conversely, model A, featuring amine-adduct cured pure epoxy, exhibits higher values. Model C, which incorporates glass flakes for reinforcement, demonstrates moderate levels of residual stress. These findings underscore the significance of curing conditions and coating thickness in determining residual stress profiles in epoxy coatings.

ACKNOWLEDGEMENTS

The author would like to thank the staff at Material Science Department, College of Engineering, Baghdad University for helping to achieve X-ray measurements.

COMPETING INTERESTS

The author declares that there is no conflict of interest regarding the publication of this article.

REFERENCES

[1] A.J. McGinnis, T.R. Watkins, K. Jagannadham (1999), "Residual stress measurement in multilayer system of coatings", *Ad. in X-ray Analy.*, **41**, pp.443-454.

[2] R.P. Anthony (1992), *A Study of Residual Stress Formation in Three Dimensionally Constrained Epoxy Resins*, Ph.D. Thesis, University of Massachusetts, USA, 178pp.

[3] V. Antonucci, A. Cusano, M. Giordano, et al. (2006) "Cure-induced residual strain build-up in a thermoset resin", *Composites*, **37(4)**, pp.592-601, DOI: 10.1016/j.compositesa.2005.05.016.

[4] H. Windischamann, G.F. Epps, Y. Cong, et al. (1991), "Collins, intrinsic stress in diamond films prepared by microwave plasma CVD", *J. Appl. Phys.*, **69(4)**, pp.223l-2237, DOI: 10.1063/1.348701.

[5] Y. Fu, H. Du, C.Q. Sun (2003), "Interfacial structure, residual stress and adhesion of diamond coatings deposited on titanium", *Thin Solid Films*, **424(1)**, pp.107-114, DOI: 10.1016/S0040-6090(02)00908-2.

[6] M.E. Fitzpatrick, A.T. Fry, P. Holdway, et al. (2005), "Determination of residual stresses by X-ray diffraction - Issue 2", *Measurement Good Practice Guide No. 52*, 78pp.

[7] M. Heidari (2015), "Estimation of residual stresses in thick walled cylinder by radial basis artificial neural", *Mech. and Mechatronics Eng.*, **2(8)**, pp.93-104.

[8] D. Umbrello, G. Ambrogio, L. Filice, et al. (2008), "Hybrid finite element method-artificial neural network approach for predicting residual stresses and the optimal cutting conditions during hard turning of AISI 52100 bearing steel", *Materials and Design*, **29(4)**, pp.873-883, DOI: 10.1016/j.matdes.2007.03.004.

[9] I.V. Manoj, H. Soni, S. Narendranath, et al. (2022), "Examination of machining parameters and prediction of cutting velocity and surface roughness using RSM and ANN using WEDM of altemp HX", *Advances in Materials Science and Engineering*, **2022**, pp.1-9, DOI: 10.1155/2022/5192981.

[10] F. Kara, M. Karabatak, M. Ayyıldız, et al. (2020), "Effect of machinability, microstructure and hardness of deep cryogenic treatment in hard turning of AISI D2 steel with ceramic cutting", *J. Mater Res Technol.*, **9(1)**, pp.969-983, DOI: 10.1016/j.jmrt.2019.11.037.

[11] P. Kamarchik, G.P. Cunningham (1980) "Application of X-ray technique to coating analysis", *Progress in Organic Coatings*, **8(1)**, pp.81-107, DOI: 10.1016/0300-9440(80)80005-1.

[12] I. Kishore (2003), "Residual stress in metal epoxy system", *MIE 605 Term Project Introduction to Finite Element Method*, University of Massachusetts, USA, 4pp.

[13] S.B. Aboubakar (2009), "Evaluation axisymmetric analysis of thermal stress residual near fiber/epoxy interface", *Material Research*, **12(2)**, pp.133-137, DOI: 10.1590/S1516-14392009000200004.

[14] J. Cheng, J. Li, J.Y. Zhang (2009), "Curing behavior and thermal properties of trifunctional epoxy resin cured by 4, 4'-diaminodiphenyl sulfone", *EXPRESS Polymer Letters*, **3(8)**, pp.501-509, DOI: 10.3144/expresspolymlett.2009.62.

[15] M. Frantisek, M. Marcel, C.G.P. Cardona, et al. (2014), "Residual stress prediction using neural network approaches", *Applied Mechanics and Material*, **611(1)**, pp.436-440, DOI: 10.4028/www.scientific.net/AMM.611.436.

[16] D. Taisei, N. Masyuki, O. Juinchi (2015), "Residual stresses measurement of industrial polymer by X-ray diffraction", *Advance Material Research*, **1110(1)**, pp.100-103, DOI: 10.4028/www.scientific.net/AMR.1110.100.

[17] Q. Li, C.E. Weinell, S. Kii (2022), "Curing-induced internal stress in epoxy coatings: Effects of epoxy binder, curing agent, filler, initial solvent concentration, curing temperature, and relative humidity", *Progress in Organic Coat.*, **173**, DOI: 10.1016/j.porgcoat.2022.107175.

[18] ASTM (2010), *ASTM-E0915-96R02 Test Method for Verifying The Alignment of X-ray Diffraction Instrumentation for Residual Stress Measurement*, https://www.astm.org/e0915-96r02.html, accessed 15 September 2022.

[19] ASTM (2020), *Standard Specification for Pressure Vessel Plates, Heat-Treated, Carbon-Manganese-Silicon Steel*, https://www.astm.org/a0537_a0537m-20.html, accessed 15 September 2022.

[20] O. Anderoglu (2004), *Residual Stress Measurement using X-ray Method*, MSc. Thesis, Mechanical Department, Texas A&M University, USA, 76pp.

[21] C.P. Gazzara (1983), "The measurement of residual stress with X-ray diffraction", *Report of Army Material and Mech. Research Center, Massachusetts, USA*, 49pp.

[22] C. Suryanarayana, M.G. Norton (1998), *X-Ray Diffraction A Practical Approach*, Springer, DOI: 10.1007/978-1-4899-0148-4, 273pp.

[23] ASTM (2012), *Standard Test Methods for Tension Testing of Metallic Materials*, https://www.astm.org/e0008_e0008m-09.html, accessed 15 September 2022.

[24] ASTM (2022), *Standard Test Method for Tensile Properties of Plastics*, https://www.astm.org/d0638-14.html, accessed 15 September 2022.

[25] Simu Tech Group (2015), *Extreme Thermal Expansion Modelling in ANSYS Mechanical*, https://simutechgroup.com/extreme-thermal-expansion-modeling-in-ansys-mechanical-workbench/, accessed 15 September 2022.

[26] Ö. Erkan, B. Işık, A. Çiçek, et al. (2013), "Prediction of damage factor in end milling of glass fiber reinforced plastic composites using artificial neural network", *Appl. Compos. Mater.*, **20**, pp.517-536, DOI: 10.1007/s10443-012-9286-3.

[27] ASTM (1986), *Test Method for Linear Shrinkage of Cured Thermosetting Casting Resins during Cure*, https://global.ihs.com/doc_detail.cfm?document_name=ASTM%20D2566&item_s_key=00016731, accessed 15 September 2022.

[28] Y. Nawab, S. Shahid, N. Boyard, et al. (2013), "Chemical shrinkage characterization techniques for thermoset resins and associated composites", *J. of Mat. Sci.*, **48(16)**, pp.5387-5409, DOI: 10.1007/s10853-013-7333-6.

[29] K. Magniez, A. Vijayan, N. Finn (2012), "Apparent volumetric shrinkage study of RTM6 resin during the curing process and its effect on the residual stresses in a composite", *Polymer Engineering and Science*, **52(2)**, pp.346-351, DOI: 10.1002/pen.22088.

[30] Hempel (2018a), *Hempadur 15600*, https://www.hempel.com/vi-vn/products/hempadur-15600-15600, accessed 15 September 2022.

[31] Hempel (2018b), *Hempadur 85671*, https://www.hempel.com/vi-vn/products/hempadur-85671-85671, accessed 15 September 2022.

[32] Hempel (2018c), *Hempadur Multi-Strength GF 35870*, https://www.hempel.com/products/hempadur-multi-strength-gf-35870-35870, accessed 15 September 2022.

[33] J.A. Ramos, N. Pagani, C.C. Riccardi, et al. (2005), "Cure kinetics and shrinkage model for epoxy-amine systems", *Polymer*, **46(10)**, pp.3323-3328, DOI: 10.1016/j.polymer.2005.02.069.

[34] Y. Mei (2000), *Stress Evolution in a Conductive Adhesive During Curing and Cooling*, Ph.D. Thesis, Rackham School of Graduate Studies, University of Michigan, 164pp.

[35] S. Song, K.W. Shahwan, A.M. Waas, et al. (2007), "Braided textile composites under compressive loads: Modeling the response, strength and degradation", *Composite Sci. Technol.*, **67(15-16)**, pp.3059-3070, DOI: 10.1016/j.compscitech.2007.06.008.

[36] C. Li (2017), *Measurement and Understanding of The Residual Stress Distribution as a Function of Depth in Atmosphere Plasma Sprayed (APS) Thermal Barrier Coatings*, Ph.D. Thesis, School of Materials, Faculty of Science and Engineering, University of Manchester, USA.

[37] E.D. Wetzel, S.R. White (2004), "Review of Soviet/Russian literature on residual stress development in filament-wound polymer-matrix composites", *Report of Army Research Laboratory, Aberdeen Proving Ground, MD 21005-5069*, 41pp.

[38] S. Chang (2015), *Cure Kinetics Study of Two Part Epoxy Resin and The Effect on Characterization of Thermal Barrier Coatings*, M.Sc. Thesis, Materials Science and Engineering Department, Virginia Polytechnic Institute and State University, USA, 94pp.